Mechanical characterization of an interpenetrating metal-matrix-composite based on highly homogeneous ceramic foams

J. Schukraft[1], C. Lohr[1], K. A. Weidenmann[1]
[1]Institute for Materials Resource Management, Augsburg University

1 Abstract

In this study an interpenetrating metal-matrix-composite of a highly homogeneous alumina ceramic foam and an AlSi10Mg aluminum alloy, fabricated via gas pressure infiltration of the ceramic preform with the molten aluminum alloy is investigated mechanically. This composite shows promising mechanical properties compared to other interpenetrating aluminum-alumina composites due to its ceramic preform and manufacturing process. To get an understanding of the application potential and limits of this material, mechanical characterization is carried out in a compression test combined with an in-situ method of a digital microscope to analyze the failure mechanism and crack propagation during compression tests. The received results from this study are compared with other studies in this field to place this new material into the range of investigated interpenetrating phase composites (IPCs) based on aluminum-alumina composites.

2 Introduction

Light-weight materials for structural application play a key role in nowadays engineering success regarding the reduction of greenhouse gases and environmentally compatible implementations in mobility and transportation. The limits of light weight metals are reached mainly for mechanical load in an environment under elevated temperature. In this area of application, metal-matrix-composites (MMC) and especially interpenetrating phase composites show a great potential [1]. By combining ceramic structures with a metallic phase in an interpenetrating microstructure, each phase contributes to the macroscopic properties of the composite which gives the opportunity to tune the properties or also develop multifunctional materials [2]. Aluminum based MMCs are in special focus of research regarding their properties and potential. Therefore aluminum is the most utilized metallic alloy in the MMC development [3]. Infiltrating sintered ceramic preforms with a metallic phase is the most common used manufacturing method for interpenetrating composites [2, 4–7]. An overview of research on various manufactured IPCs based on aluminum-alumina, are given in **Table 1** with ceramic content, range of pore size in the ceramic phase, type of aluminum alloy used for the metallic phase, compressive strength, strain rate and elongation at compression strength as far as specified in the publications.
The mechanical properties as well as the microstructure of the composite is mainly based on the ceramic preform. For an isotropic mechanical behavior, a homogeneous pore distribution within the ceramic without a geometrically predominant direction, is required. Colombo and Bernardo [8] have shown the microstructural need of a small pore size for a mechanically durable ceramic foam. Previous microstructural investigations via X-ray computed tomography have shown a narrow pore-size distribution with open, homogeneous and spherical pores and dense ceramic struts in the ceramic foam investigated here [9].

Table 1. Overview of different interpenetrating ceramic metal composites of alumina and aluminum alloys from literature.

ceramic phase manufacturing method	ceramic content	pore size	type of metal	residual porosity	compression strength	strain rate	elongation at compression strength/break	publication
[-]	[%]	[µm]	[-]	[%]	[MPa]	[-]	[%]	[-]
freeze casting / pore former	35 - 40	NSF	AlSi12	NSF	500 – 900	NSF	0,01 - 10	[10]
freeze casting	43 ± 2	NSF	AlSi12	NSF	270 - ca. 700**	10^{-3} 1/s	2,5 - 10	[11]
pyrolysable placeholder	24,3	NSF	AlSi12	NSF	277*	NSF	NSF	[12]
pyrolysable placeholder	29,5	NSF	AlSi12	NSF	301,5*	NSF	NSF	[12]
hollow alumina particle	NSF	NSF	AlSi7Mg0,3	NSF	up to 275	10^{-3} 1/s	NSF	[13]
replica technique	30,57	300 - 450	AlSi12CuMgNi	0,57	341	NSF	ca. 4	[14]
replica technique	28,52	450 - 550	AlSi12CuMgNi	1,6	317	NSF	ca. 4	[14]
replica technique	25,58	800 - 1000	AlSi12CuMgNi	1,44	294	NSF	ca. 4	[14]
gelcasting of foams	10	500	AlMg5	<1	320	NSF	0,09	[15]

NSF = Not specified

* Tensile, no compression values available

** lowest value for 34 ° angle to freeze direction, highest value in freezing direction tested

3 Experimental/ Materials and Methods

For the experiments, a macroscopic homogeneously and highly porous open-cell alumina ceramic foam, with an approximate relative density of 25 %, provided by Morgan Advanced Materials Haldenwanger GmbH, Waldkraiburg, Germany is used, who hold a patent on the low-cost manufacturing technique [16]. An interpenetrating metal ceramic composite is produced via gas pressure infiltration based on the ceramic foam and an AlSi10Mg aluminum alloy, as described by the authors [9]. The materials were cut into cubic samples of ca. 5 x 5 x 5 mm³ and the sample surface was grinded stepwise with silicon carbide paper up to grain size P800, with water as coolant.
For in-situ microscopy one cube-surface also was polished with diamond suspensions (9, 3 and 1 µm) and OP-S-Suspension, each manufactured by Struers, Friedberg, Germany.

Compression tests were carried out with a universal testing machine of type 1464, with a load cell xforceK up to 50 kN, each of Zwick&Roell, Ulm, Germany. Interchangeable compression stamps with plane turned and then polished end faces (SiC grinding paper with grain size up to P4000 and water as coolant) were made of hardened machine screws of grade 12.9 with tensile strength of 1200 N/mm² and a yield strength of 1050 N/mm². Molybdenum sulfide (OKS Spezialschmierstoffe GmbH, Munich, Germany) was used as a solid lubricant between the sample and the stamps in accordance to DIN 50106 [17]. A preload of 20 N was applied onto the sample, before the data logging started. The strain rate during the compression tests was set to 10^{-3} 1/s. Abort criterions for the experiments were set for a minimum stamp distance of 3 mm and a drop in maximum force of 80 %. Three samples were tested with the in-situ testing. Therefore, load steps were integrated into the compression test procedure at stresses of 250, 300, 340, 360 and 380 MPa for the composite.
For optical elongation determination the ARAMIS Adjustable System with two 12 Megapixel cameras by GOM, Braunschweig, Germany was used. For the specific setup, lenses with a focal

length of 100 mm and one polar filter for each camera were used. The working distance between camera and sample was ca. 50 cm and two LED spotlights were used for the uniform illumination of the sample. A black and white speckle pattern was applied on the sample surface examined with the ARAMIS-System.
A digital microscope of type VHX-600 by Keyence, Neu-Isenburg, Germany was installed with a 50 to 500 x magnification (VH-Z50L, Keyence) on the opposite side of the sample, to investigate the damage behavior and the crack propagation during the compression test. The complete test setup of the in-situ compression tests is shown in **Figure 1**:

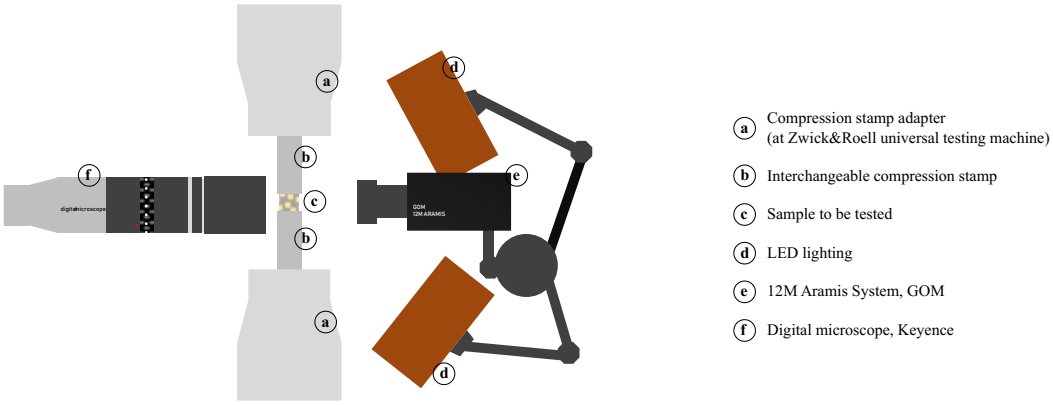

Figure 1. In-situ testing setup: Zwick&Roell universal testing machine, GOM ARAMIS Adjustable 12M System and Keyence digital microscopy.

4 Results and Discussion

The results of the compression tests for the ceramic preform are shown in **Figure 2**. The elongation has been tracked with the Aramis GOM-System, based on a speckle pattern. At the point of failure, the speckle pattern can spall from the brittle surface or because of spontaneous big displacements, the software is not able to calculate the elongation correctly anymore. Therefore, the values are just plotted until the point of failure. The curves were also smoothed with a Lowess algorithm.

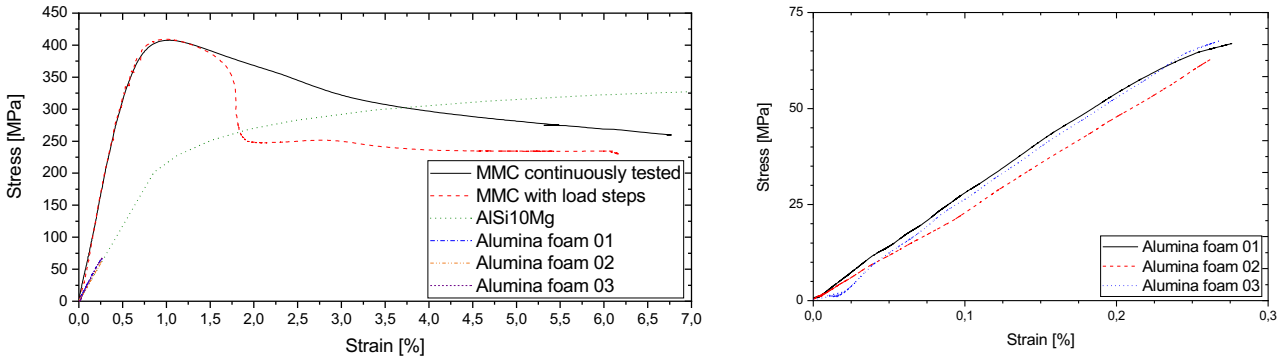

Figure 2. *Left:* Stress-strain diagram of the compression test with a strain rate of $\dot{\varepsilon} = 10^{-3}$ 1/s for the alumina ceramic foam, the produced interpenetrating composite and an AlSi10Mg alloy (values taken from literature [20]).
Right: Enlarged visualization of the results for the ceramic foam.

The ceramic foam shows a linear behavior until failure and has an elongation at break higher than 0,25 %, which is more than twice the elongation at break of a dense alumina ceramic [18]. The compression strength of this ceramic foam lies between 60 and 65 MPa. Compared to some other studies on alumina based ceramic foams with a comparable porosity, produced in different ways, the

investigated ceramic foam has a higher compressive strength. Hadi et al. [19] produced a ceramic foam via replica technique with a porosity of 80 – 83 % and 14 pores per inch. The compressive strength of their foam reached 1,33 – 3,24 MPa. Prabhakaran et al. [20] used a pore-former process for their material with 67 – 76,7 % porosity and a bimodal pore size distribution in the range of 20 µm and 200 – 800 µm. They reached a compressive strength of 2,01 – 5,9 MPa for their material. Vijayan et al. [21] investigated a freeze gel-casting foam with 70 % porosity and an average pore size of 13,24 µm with a compressive strength of 39,6 MPa. Tallon et al. [22] investigated alumina foams produced via stabilized foams and gel casting process in a varying range of porosity between 65 – 93 %. They reached for small pore size between 100 and 150 µm a compressive strength of 57,8 MPa at a porosity of 63 %. For bigger pores around 300 µm they determined lower compressive strengths. Colombo et al. [8] showed a dependency of mechanical strength of the ceramic foams on the pore size. For small pores (8 µm) they determined a two to five times higher compressive strength than for bigger pores (100 – 600 µm). In the mentioned examples from literature, it becomes obvious, not only the pore size is responsible for the mechanical stability of ceramic foams. The microstructure resulting from the respective manufacturing process also plays a decisive role for the mechanical strength. For replica technique e.g., the ceramic struts often show pores inside, like it can be seen exemplarily in the following publications by Hadi et al. [19], Accher et al. [23], Boczkowska [24] and Dolata [25]. Studart et al. [26] give an overview of different ceramic foams, in which the compressive strength is shown as a function of porosity and the manufacturing process. The alumina foam of the present study can be placed in the upper area of the compressive strength of the open porous alumina foams within their diagram, which spans from 0,15 to 100 MPa (for relative densities from 0,04 to 0,54). The highly homogeneous pore distribution inside the ceramic and the dense ceramic struts as well as the narrow pore-size distribution with a low median pore diameter of approximately 20 µm [9] are microstructural reasons for the foam having such high load capacity.

As an example, **Figure 2** shows two stress-strain curves of the composite in addition to the curves of the ceramic foam. One curve shows the course of the compression testing with constant strain rate (*MMC continuously tested*). The other curve shows the course where load steps were implemented for the in-situ investigations of the sample (*MMC with load steps*). For the *MMC with load steps* the test was terminated when a certain number of images was reached with the GOM-System. The experiment of the *MMC continuously tested* was terminated after a significant stress decrease from the maximum stress. The curves of the two compression tests correspond very well up to the maximum stress, where the ceramic phase fails with an audible cracking. The maximum compression strength is approximately 407 MPa. The further course of the *MMC with load steps* is different from the *MMC continuously tested* and shows a drop in stress. Reasons for that could be local failure of ceramic struts or microscopic crack growth in the ceramic phase during the load steps in combination with dislocation slip as well as dislocation creep in the metallic phase for high stresses, also occurring during the load steps, but this phenomenon is not finally investigated yet and the given reasons are just thesis which have to be proved. Also remarkable is the three times higher elongation in the composite at maximum compression stress in comparison with the ceramic foam (approximately 1 % compared with 0,25 % elongation at break), what can also be seen in other publications, like Boczkowska et al. [14] e.g. For the classification of the compressive strength of the composite, values from other publications were compiled in **Table 1**.

The compression stress-strain curve of a bulk AlSi10Mg alloy is shown in **Figure 2** for the same range of elongation. The data of the curve progression are cut of at the elongation of 7 % for a better overview and been obtained from Stanev et al. [27], who based their figure on Stanev et al. [28]. Due to the ceramic interpenetrating phase, the composite is significantly stiffened compared to the aluminum alloy and also gains in strength. The brittle material properties of the ceramic are

compensated largely by the metallic phase, as the course of the composite shows in **Figure 2** in comparison to the original materials of which the phases of the composite are made.

Representative micrographs of the sample, which is shown in the stress-strain diagram in **Figure 2** (*MMC with load steps*), are shown in **Figure 3** for the condition under preload and at the end of the compression test. The material contrast between metal and ceramic made a good differentiation of the phases. The local plastic deformation in the metallic phase as well as the crack growth in the ceramic phase, the metallic phase as well as at the phase boundaries up to macroscopically big cracks can be seen.
The experimental setup, introduced in **Figure 1**, makes additionally optical strain analysis accessible. The phenomenon of macroscopic cracks, tend to grow under ± 45 ° in the material sample, can also be detected in the optical strain analysis like the results show in the middle of **Figure 3** in comparison to the micrograph in the right part. The strain orthogonal to the load direction shows also concentration along ± 45 ° according to the load direction. This gives first indications to a shear driven failure mechanism in the section of decreasing stress after the maximum compression stress was reached and the main load-bearing structure of the ceramic phase has failed with an audible crack. But for consideration of the entire range of failure, the complex interpenetrating material structure shows a complex failure process with a multidirectional crack growing progress. Thereby a clear failing mechanism could not be determined yet. This shows that a two-dimensional investigation of crack growth and failure mechanism at the sample surface is not enough to get an understanding of the complete failure mechanism in this interpenetrating phase composite.

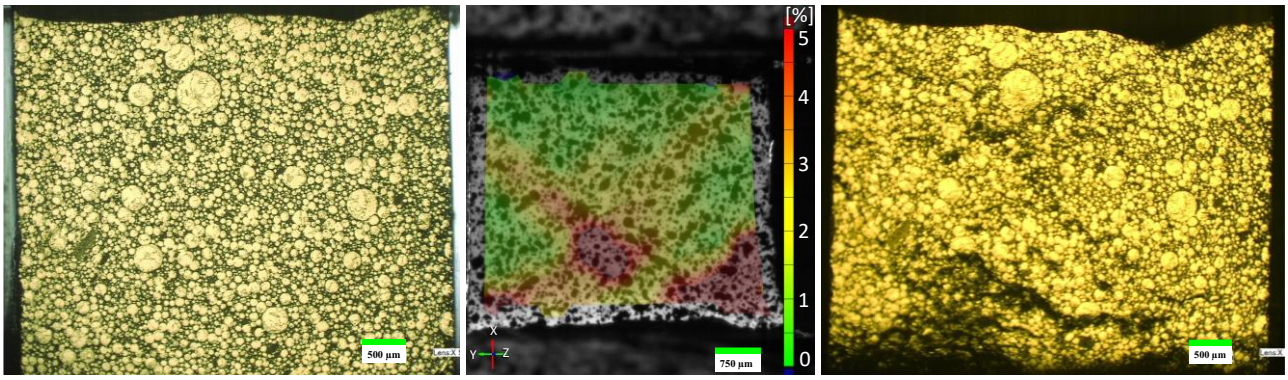

Figure 3. Micrographs of in-situ compression test. Overview of the sample "*MMC with load steps*" with preload (*left*) and at the end of the test (*right*), strain in Y-direction at one of the last images with full pattern identification of the software (*middle*). Strain scale is cut off at 5 % to illustrate the elongation course over the surface. Local maximum strains up to 15 % are reached in the lower right corner.

5 Conclusion/Summary and Outlook

Compression tests on an interpenetrating metal-ceramic composite and on a homogeneous ceramic foam, the composite is based on, were carried out successfully. The compression tests show a high load capacity of the ceramic foam (60 – 65 MPa) due to its well-developed microstructure for mechanical application. This property is also reflected in the composite, where high stiffness and high compression strength (407 MPa) can be seen. At the same time, the metallic phase compensates the brittle properties of the ceramic foam and the elongation at maximum compression stress of the MMC is three times higher than the elongation at break of the ceramic foam.

Furthermore, an in-situ setup was presented, to investigate two-dimensional crack growth and failure at the sample surface during compression testing. The method is especially suitable for composite materials with a good optical contrast.
This work also showed fist results of crack growth at the surface of the interpenetrating aluminum-alumina composite. Because of the complex microstructure and load distribution inside the composite specimen, further investigations with three-dimensional in-situ methods (e.g. computed tomography) will be conducted to fully understand the failure mechanisms of interpenetrating composite structure.

6 Acknowledgements

The financial support for this work in the context of the DFG research project WE 4273/17 is gratefully acknowledged. We also want to thank Morgan Advanced Materials Haldenwanger GmbH for the friendly supply of material samples of the ceramic foam, used in this work.

7 References

[1] Clarke, D. R., *J. Am. Ceram. Soc.* **1992**, 4, 739–758.

[2] Peng, H. X., Fan, Z. und Evans, J.R.G., *Materials Science and Engineering: A* **2001**, 303, 37–45.

[3] Bodunrin, M. O., Alaneme, K. K. und Chown, L. H., *Journal of Materials Research and Technology* **2015**, 4, 434–445.

[4] Scherm, F., Völkl, R., Neubrand, A., Bosbach, F. und Glatzel, U., *Materials Science and Engineering: A* **2010**, 4-5, 1260–1265.

[5] Roy, S. et al., *Materials Science and Engineering: A* **2011**, 28, 8226–8235.

[6] Binner, J., Chang, H. und Higginson, R., *Journal of the European Ceramic Society* **2009**, 5, 837–842.

[7] San Marchi, C., Kouzeli, M., Rao, R., Lewis, J. A. und Dunand, D. C., *Scripta Materialia* **2003**, 49, 861–866.

[8] Colombo, P., *Composites Science and Technology* **2003**, 16, 2353–2359.

[9] Horny, D., Schukraft, J., Weidenmann, K. A. und Schulz, K., Submitted to *Advanced Engineering Materials,* **December 2019.**

[10] Roy, S., Gibmeier, J., Weidenmann, K. A., Nagel, A. und Wanner, A. in W. Udomkichdecha, T. Böllinghaus, A. Manonukul und J. Lexow, Hg., Cham: Springer International Publishing, **2014**, 77–86.

[11] Roy, S., Butz, B. und Wanner, A., *Acta Materialia* **2010**, 7, 2300–2312.

[12] Dobrzanski, L. A., Kremzer, M., Nowak, A. J. und Nagel, A.*, Archieves of Materials Science and Engineering* **2009**, 1, 5–11.

[13] Licitra, L., Luong, D. D., Strbik, O. M. und Gupta, N.*, Materials & Design* **2015**, 504–515.

[14] Boczkowska, A. et al.*, SSP* **2012**, 57–66.

[15] Potoczek, M. und Śliwa, R.*, Archives of Metallurgy and Materials* **2011**, 4, 41.

[16] Lavrentyeva, O. DE. Patent DE102015202277A, **2016.**

[17] *Prüfung metallischer Werkstoffe - Druckversuche bei Raumtemperatur*, DIN 50106:2016-11, **2016**.

[18] *CES EduPack,* GRANTA DESIGN, **2019**.

[19] Hadi, A., Emadi, R., Baghshahi, S. und Naghavi, S. H.*, Ceramics - Silikaty* **2015**, 90–95.

[20] Prabhakaran, K., Melkeri, A., Gokhale, N. M. und Sharma, S. C.*, Ceramics International* **2007**, 1, 77–81.

[21] Vijayan, S., Narasimman, R. und Prabhakaran, K.*, Journal of the European Ceramic Society* **2014**, 16, 4347–4354.

[22] Tallon, C., Chuanuwatanakul, C., Dunstan, D. E. und Franks, G. V.*, Ceramics International* **2016**, 7, 8478–8487.

[23] Acchar, W. et al.*, J Mater Sci* **2008**, 19, 6556–6561.

[24] Boczkowska, A., Chabera, P., Dolata, A. J., Dyzia, M. und Oziębło, A.*, Metalurgija* **2013**, 3, 345–348.

[25] Dolata, A. J.*, Journal of Materials Engineering and Performance* **2016**, 8, 3098–3106.

[26] Studart, A. R., Gonzenbach, U. T., Tervoort, E. und Gauckler, L. J.*, J. Am. Ceram. Soc.* **2006**, 6, 1771–1789.

[27] Stanev, L., Kolev, M., Drenchev, B. und Drenchev, L.*, Journal of Manufacturing Science and Engineering* **2017**, 5, 810.

[28] Stanev, L., Drenchev, B., Yotov, A., and Lazarova, R.*, Journal of Materials Science and Technology* **2014**, 1, 44–53.